Research Article

Molecular modeling-based evaluation of dual function of IκBζ ankyrin repeat domain in toll-like receptor signaling

Balachandran Manavalan[a], Rajivgandhi Govindaraj[a], Gwang Lee[a,b] and Sangdun Choi[a]*

IκBζ (inhibitor of NF-κB (nuclear factor κB) ζ) is a nuclear protein induced upon stimulation of toll-like receptors (TLRs) and interleukin-1 receptor. Induced IκBζ, especially its C-terminal ankyrin repeat domain (ARD), interacts with NF-κB in the nucleus, where it regulates the transcriptional activity of target genes. Recent studies have shown that human ARD of IκBζ binds with p50/p65 heterodimer and inhibits the transcription of NF-κB regulated genes, whereas mouse ARD of IκBζ binds with p50/p50 homodimer and exhibits transcriptional activation activity. Since human and mouse IκBζ ARD are identical, it is unclear how IκBζ can be a positive and negative regulator of NF-κB-mediated transcription. Therefore, we generated a structural model of IκBζ ARD and constructed a detailed molecular dynamics (MD) simulation of IκBζ in explicit solvent to investigate ARD flexibility. In addition, we used molecular docking to screen for potential sites of interaction between IκBζ and the p50/p65 heterodimer and IκBζ and the p50/p50 homodimer. The docking experiments revealed that the binding of IκBζ ankyrin repeats with the p50/p65 N-terminal DNA binding domain prevents NF-κB-mediated transcriptional activation. Furthermore, the IκBζ–p50 homodimer complex, which lacks Pro, Glu (and Asp), Ser and Thr (PEST motif), facilitated gene expression. These two different binding schemes of IκBζ may be responsible for its opposite function, which is consistent with the currently available biochemical data. Moreover, our data implicate structurally highly flexible ARD residues as the prime contributors to this dual function. Copyright © 2010 John Wiley & Sons, Ltd.

Supporting information may be found in the online version of this paper.

Keywords: IκBα; IκBζ ARD; NF-κB; protein–protein docking; toll-like receptor

INTRODUCTION

Nuclear factor kappa B (NF-κB) is a major regulator of innate and adaptive immunity, apoptosis, cell proliferation, and differentiation. The mammalian NF-κB family consists of p65 (or RelA), RelB, c-Rel, p50 (or NF-κB1), and p52 (or NF-κB2), which bind to the κB sites in the DNA of their target genes as homo- or heterodimers through the conserved Rel homology domain (RHD). The p65, RelB, and c-Rel subunits contain a transcriptional activation domain at their C-terminal end, which is not a part of p50 and p52. Therefore, the p50/p65, p65/c-Rel, and RelB/p52 heterodimers act as transcriptional activators and homodimers of p50 or p52, which repress transcription (Siebenlist *et al.*, 1994; Hayden and Ghosh, 2004). In unstimulated cells, NF-κB dimers localize in the cytosol through association with the IκB family of proteins. The IκB protein family comprises three functional groups: (a) the typical IκB proteins, namely IκBα, IκBβ, and IκBε, which are present in the cytoplasm of unstimulated cells and undergo stimulus induced degradation and resynthesis; (b) the precursor proteins p100 and p105, which can be processed to form NF-κB family members p52 and p50, respectively; and (c) the atypical IκB proteins, namely IκBζ, Bcl-3, and IκBNS, which are not generally expressed in unstimulated cells, but are induced upon activation and mediate their effects in the nucleus (Hayden and Ghosh, 2008).

IκBα is the prototypical member of the IκB family. Following activation of cells with the appropriate stimuli, the cytosolic IκBα becomes phosphorylated and undergoes rapid ubiquitin–

proteasomal degradation that results in the release of NF-κB dimers. These liberated dimers then translocate into the nucleus and bind to the promoter/enhancer of target genes, which regulate transcription through the recruitment of coactivators and corepressors (Ghosh *et al.*, 1998; Hatada *et al.*, 2000). The principal regulators of NF-κB are IκB proteins, which share a common C-terminal structural motif that is essential for their function, the ankyrin (ANK) repeat domain (ARD). Most members of the IκB family have 6–7 ARDs that each consists of 33 amino acid residues and forms an L-shaped structure having two α-helices separated by a loop. The repeated structural motifs stack one upon another in a linear fashion to form a curve shaped

---

* Correspondence to: S. Choi, Department of Molecular Science and Technology, Ajou University, Suwon 443-749, Korea.
  E-mail: sangdunchoi@ajou.ac.kr

a B. Manavalan, R. Govindaraj, G. Lee, S. Choi
  Department of Molecular Science and Technology, Ajou University, Suwon 443-749, Korea

b G. Lee
  Institute for Medical Sciences, Ajou University School of Medicine, Suwon 443-749, Korea

architecture (Sedgwick and Smerdon, 1999). These motifs are known to facilitate the protein–protein interactions, but have no known enzymatic activity (Mosavi *et al.*, 2004). These types of structural motifs are involved in various biological functions, such as transcriptional regulation, cytoskeletal organization, the cell cycle, cell development, and differentiation (Forrer *et al.*, 2003; Main *et al.*, 2003). The carboxyl terminal of ARD is rich in proline, glutamic acid, serine, and threonine (PEST). The acidic PEST sequence has long been recognized as an element common to proteins that display rapid turnover in the cell (Rogers *et al.*, 1986). However, the role of the ankyrin domain and the C-terminal PEST sequence have been shown to be essential for interactions with the NF-κB dimer and its subsequent removal from the DNA (Ghosh *et al.*, 1998; Jacobs and Harrison, 1998; Malek *et al.*, 1998).

IκBζ, which was discovered independently in three laboratories (Kitamura *et al.*, 2000; Haruta *et al.*, 2001; Yamazaki *et al.*, 2001), has a high degree of homology with Bcl-3 and has been described as a regulator of NF-κB. In mice, there is no expression of IκBζ in the resting state and it is induced by lipopolysaccharide (LPS), interleukin-1 beta (IL-β), peptidoglycan, bacterial lipoprotein, flagellin, and C_pG DNA, but not by tumor necrosis factor alpha (TNFα) (Yamazaki *et al.*, 2001; Yamamoto *et al.*, 2004; Motoyama *et al.*, 2005). Conversely, human IκBζ expression is strongly induced by TNFα (Totzke *et al.*, 2006). Stimulation with TLR ligands results in the production of three different alternative splicing variants of IκBζ: L, S, and D. IκBζ (L) is predominantly expressed in response to LPS stimulation (Kitamura *et al.*, 2002; Yamazaki *et al.*, 2005), while expression of IκBζ (S) has been observed at the mRNA and protein levels in minor species (Yamazaki *et al.*, 2005). Although IκBζ (D) mRNA has been detected in macrophages, the corresponding protein has not been found. Following induction, IκBζ associates with the NF-κB subunit in the nucleus, where it positively or negatively regulates its transcriptional activity (Motoyama *et al.*, 2005). Previous biochemical studies suggest that following the endogenous expression of mouse IκBζ in response to LPS, IκBζ is translocated into the nucleus, where it preferentially associates with the p50/p50 homodimer of NF-κB, which is already bound to DNA. In this ternary complex, IκBζ transforms the inactive NF-κB p50/p50 homodimer into a competent activator of transcription, which results in augmentation of IL-6 production. Furthermore, recent studies have indicated that human TNFα-induced IκBζ becomes associated with both the p65 and p50 subunits of NF-κB in the nucleus, and subsequently inhibits the transcriptional activity of antiapoptotic proteins (Totzke *et al.*, 2006). Wet lab experiments have shown that human IκBζ binds to the p50/p65 heterodimer, while mouse IκBζ shows a preference for p50/p50 homodimer. Because it is evident that only C-terminal ARD (452–718) is capable of binding with its partners (Yamazaki *et al.*, 2001; Motoyama *et al.*, 2005; Totzke *et al.*, 2006), we have concentrated solely on the C-terminal ARD in the present study.

In this study, we used a combination of homology modeling and molecular dynamics (MD) simulation to construct a detailed three-dimensional (3D) model of IκBζ to identify and quantify the structural flexibility of ARD. The 3D model was then used to investigate the nature of the two different binding modes with the p50/p65 hetero and p50/p50 homodimer of the NF-κB subunits. The two complex structures were studied to analyze the intermolecular contacts and to identify the specific residual level of interactions between the two proteins. The results showed that two entirely different orientations are possible, in agreement with the experimental findings. In addition, the findings presented here provide an explanation for the dual functions of IκBζ ARD. We also identified the structural flexibility of IκBζ, which is the major contributor to its dual nature. These data will be useful to direct further mutagenesis studies to investigate their effects on binding activity. Here, we provide detailed information regarding the model of IκBζ–NF-κB complexes and offer a structural interpretation of the available experimental data.

MATERIALS AND METHODS

Homology modeling

The primary sequences of human and mouse IκBζ share 70% identity with the N-terminal region (1–454) and 97% identity with the C-terminal ARD (455–725) (Yamazaki *et al.*, 2001; Totzke *et al.*, 2006). Previously conducted biochemical studies have shown that C-terminal ARD was sufficient to bind with its partners such as p50 homo and p50/p65 hetero dimer. Therefore, we used the C-terminal ARD domain primary sequence for modeling. Since IκBζ ARD is identical in mice and humans, we used the mouse sequence for the current study. The mouse IκBζ FASTA sequence (NP_085115) and crystal structure coordinates of human Bcl-3 (PDB ID: 1K1A) (Michel *et al.*, 2001) were loaded into the Molecular Operating Environment (MOE 2008.10; Chemical Computing Group, Ryoka systems Inc, Japan), after which MOE-Align was used to create target–template alignment. Subsequently, the alignment was critically inspected and the 28 amino acids residues (VAHNAVVHEL QRNRQSHSFE NRDLLLRN) within the ankyrin repeat four were deleted based on the alignment results from the Multiple Sequence Alignment (MSA) (Yamazaki *et al.*, 2001). The final target–template alignment sequence identities were 37.28%. Next, a series of 10 IκBζ models were independently constructed with MOE using a Boltzmann-weighted randomized procedure combined with logic for proper handling of the sequence insertions and deletions. There was no difference in the number of secondary structural elements and no significant main chain root mean square (RMS) deviations were found among the 10 models. However, the model with the best MOE packing score (−2.4597) was selected for full energy minimization.

MD simulation

MD simulations were conducted to assess the structural flexibility as previously described (Hariharan and Pillai, 2008) using the AMBER 99 force field distributed in MOE starting from the energy minimized IκBζ structure in each case. The MD simulation was conducted in explicit solvent and gas phase. The initial structure was inserted into a rectangular box (60.56 × 45.42 × 75.7 Å^3) while maintaining a minimum of 10 Å between the box edges and the protein surface. The resulting system was solvated with a transferable intermolecular potential three-point (TIP3P) water molecule using the MOE water soak option. The appropriate counter ions, Na^+ or Cl^-, were added to neutralize the system using the MOE pro_Neutralise option. The entire system was energy minimized until the RMSD gradient values decreased below 0.01 kcal/mol/Å. The system was heated from 0 to 300 K for 100 ps (picoseconds) and was equilibrated at 300 K for another 500 ps.

The solvation was set to gas phase in the potential control of MOE. A switching function was used for the non-bonded interaction terms in the range of 12–15 Å. This cutoff was chosen because it behaves smoothly at that point. The system was heated and equilibrated as described in the explicit solvent

method. Following minimization and heating, 5 ns (nanoseconds) production simulation was conducted with a 1 fs (femtosecond) time step at a pressure of 1 bar and a temperature of 300 K (Ponder and Case, 2003). The snapshots were collected at every 2.5 ps and analyzed using MOE. The average model was calculated for every frame in the MD trajectory between 4500 and 5000 ps (i.e., corresponding to a 500 ps trajectory) using the explicit solvent method. This average structure was compared to the MD trajectory and the structure closest to the average structure was considered to be the representative structure. A snapshot of the representative structure taken at 4245 ps was used for the structural analysis. In each case, the average structure was used as a reference to calculate the root mean square deviation (RMSD) for each amino acid during the last 2 ns MD trajectory. The RMSD calculations from the MD simulations for each case were only conducted after the protein reached an equilibrium stable state. To quantitatively assess the structural flexibilities of the ARD, the average RMSD values for each amino acid residue were taken from both simulations.

Model assessment

The overall geometric and stereochemical quality of the representative structure was assessed using PROCHECK (Lovell et al., 2003) and the Verify3Dimensional (3D) server (Eisenberg et al., 1997). A few problematic side chains (S600, Y671, and V703) were identified and corrected in the models using the rotamer explorer module in MOE. However, no gross errors or errors in packing quality were detected in our protein model.

Protein–protein docking and binding site prediction

The individual structure for docking was obtained from the dynamic structure (IκBζ), mouse p50/p65 heterodimer (PDB ID: 1VKX) (Chen et al., 1998a) and the mouse p50/p50 homodimer (PDB ID: 1NFK) (Ghosh et al., 1995) of NF-κB. The primary sequence between the human and mouse p50/p65 heterodimers were 100% identical. To explore the IκBζ interface with the human p50/p65 subunits, we utilized the 3D structure of mouse p50/p65 subunits due to lack of a human structure. Before docking, only the PDB coordinates were pre-processed for energy minimization using the AMBER 99 force field distributed in the MOE. Molecular docking was performed using the protein–protein docking software, Global Range Molecular Matching (GRAMM) (Tovchigrechko and Vakser, 2006). The GRAMM methodology is an empirical approach to smoothen the intermolecular energy function by changing the range of the atom–atom potentials. Low resolution docking is useful for determining the possible relative position of the two proteins in the complex. The program ranks the 100 most probable predictions out of thousands of candidates based on geometry, hydrophobicity, and electrostatic complementarity surface. The final docked complexes were chosen from the top 100 lists based on the available biochemical data regarding the association of human IκBζ with the N-terminal portion of the Rel homology domain (RHD) of both p50/p65 subunits (Totzke et al., 2006). As in the case of IκBζ–p50/p50 homodimer, which is solely available for the mouse model, the dimerization domain (DD) and nuclear localization signal (NLS) of p50 subunits were utilized, but not the DNA binding domain (Trinh et al., 2008). Based upon this biochemical filtering, there were 4–5 complexes (in each case) that fit into the experimental information and also possessed same orientations (Figure 3 of the Supplementary Material (S3)).

From these filtered complexes, we have chosen the final docked complex based upon the high buried surface area criterion.

The final docked complexes were subjected to energy minimization in three rounds. Partial charges were assigned to the protein after adding each of the hydrogen atoms (residues of Asp, Glu, Lys and Arg were considered ionized, while all His were considered to be neutral) by employing the AMBER 99 force field distributed in the MOE package. In the first round, constraints were applied to the heavy atoms, thereby allowing the mobility of all hydrogen atoms. In the second energy minimization round, only the backbone chain was constrained, while the side chains were allowed to move. In the third energy minimization round, only the Cα atoms were constrained, while all other atoms were allowed to move. All of the above energy minimizations were conducted using both the steepest descent and conjugate gradient protocols. The final docked complexes were defined as the residues that contain an interface solvent accessible surface area (Tina et al.), which is decreased (ΔASA) by more than 1 Å^2 upon complexation (Jones and Thornton, 1996). The ASA was calculated using the Lee and Richards algorithm (Richmond, 1984). Non-covalent interactions across the interface were calculated using the protein interaction calculator (PIC) (Tina et al., 2007).

The functional protein sequence pattern database (FPSPD) program was used to identify the functional sites (Miguel, 2004). FPSPD utilizes environment dependent substitution tables and evolutionary trace analysis to identify residues from a structurally aligned homologous family of proteins that are highly conserved. Solvent accessibility calculations (Lee and Richards, 1971) were then used to estimate the probability of residues being directly involved in the functional interactions with cofactors, substrates, and other proteins. The 3D structure of IκBζ ARD was used to estimate the borders of the functional pattern.

RESULTS

Comparative modeling of the IκBζ ARD

To generate a homology model of IκBζ ARD, we identified Bcl-3 (PDB ID: 1K1A) as the only known crystal structure of the nuclear IκB ARD family. Since the accuracy of the model primarily depends on the accuracy of the target template alignment, we used manual methods to construct the model. The ARD is a short sequence motif that typically consists of 33 amino acid residues. Generally, the insertion takes place in between the ANK repeats, which has been seen in other nuclear proteins such as IκBβ, p105, and p100 (Figure 3A). We initially modeled the IκBζ without the amino acid deletion (Figure 1 of the Supplementary Material (S1)). The 28 residues that form a long loop are located in between the helices of α1 and α2 of ANK4, which was consistent with the results of the PSIPRED secondary structure prediction (Jones and Thornton, 1996). Additionally, comparison of the modeled ANK protein (with insertion) with different ARD members did not reveal any similar insertions within the 33 amino acid long ANK repeat motif as listed in a recent review (Mosavi et al., 2004; Gaudet 2008). However, in the present study, the insertion took place within the ANK repeat. Hence, to maintain the structural integrity of the 33 amino acid long ANK repeat motif, we deleted the 28 amino acid long insertion (571–598) located between α1 and α2 of the fourth ANK repeat (Figures 1 and 3A) as it did not align with the template.

Figure 1. *Sequence alignment used to build IκBζ ARD.* The seven ANK repeats are highlighted. The arrow represents the deletion of 28 residues (VAHNAVVHEL QRNRQSHSFE NRDLLLRN). The gray block indicates the level of sequence similarity. Tallest blocks: residues are identical at that position. Intermediate blocks: residues are not identical, but relatively well conserved with respect to their properties. Small blocks: residues share mild conservation with respect to structure or function. The absence of a block indicates no appreciable structure/function conservation. Gaps in one sequence relative to the other are indicated by dots. The seven ANK repeats are highlighted and contrasted by varying the color. The UCSF chimera visualization system was used to generate this figure (Pettersen *et al.*, 2004).

The sequence alignment of IκBζ and Bcl-3, which was used to construct the model, is shown in Figure 1. The residues in the model were in environments similar to templates. A direct comparison of the ANK repeat of IκBζ and Bcl-3 revealed significant differences. Although some of the differences described below may arise from the fact that the comparison was based on the energy minimized structure, the majority of the observations are significant. Inspection of the IκBζ 3D model revealed that ANK 1, 2, 3, and 4 contained charged residues that mapped in the loop regions longer than Bcl-3, and the rest of the region was identical with a RMSD (Cα coordinates) value of 1.44 Å (Figure 2A). Surface electrostatic calculations from the homology model revealed many basic patches along with few negatively charged residues present in each of the ANK repeats of IκBζ (Figure 2B). This charged surface would bind with its targets/partners based on the respective opposite charges.

Comparison of modeled IκBζ and IκBα crystal structures

The ARD of IκBζ and IκBα (Huxford *et al.*, 1998) share 30% sequence identity over the first six ANK repeats (Figure 3A). The RMSD Cα$_{240}$ (number of Cα atoms considered to calculate the RMSD) was 2.37 Å, which demonstrates that the overall folding was similar (Figure 3B). Significant deviation was observed between the two protein backbones within the inter-helical turn of 3, 5, and 6 ANK repeats and also in between ANK repeats 3–4 and 4–5, which are represented as dots and asterisks, respectively (Figure 3B). Comparison of the structure of IκBα in its bound state to that of IκBζ revealed a significant difference at the N- and C-terminal ends. In IκBα, the N-terminal amino acid residues 71–76 adopt a β-hairpin conformation. Aspartic acid residues 73 and 75 of this β-hairpin loop interact with the basic residues (Lys301, Arg302, and Arg304) of p65, which are important for the NLS. Conversely, the N-terminus of IκBζ follows a nearly perpendicular course in which the corresponding Asp453 and

Asp455 side chains point toward an opposite direction (Figure 3C). These findings clearly demonstrate that IκBζ has no influence in p65 NLS. At the C-terminus, ANK repeat 7 of IκBζ and the PEST region of IκBα comprised approximately the same number of residues. In addition, these regions occupied a similar length, and the entire assembly lay below ANK repeat 6. However, the IκBζ turned in the opposite direction of the PEST backbone of IκBα and ended abruptly, leaving the C-termini of IκBα and IκBζ on opposite sides of the ARD (Figure 3B).
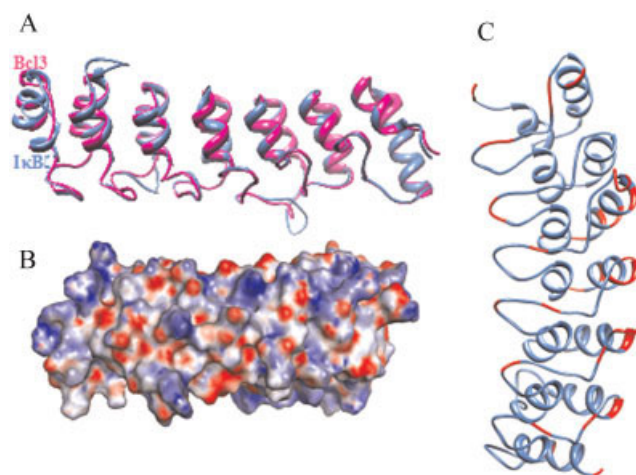
Figure 2. *Comparative modeling of the ARD of IκBζ.* (A) The superimposition of the modeled ANK repeats of IκBζ (colored in blue) with crystal structure Bcl-3 (colored in magenta). (B) Electrostatic surface of the ARD. The positively charged surface is shown in blue and the negatively charged surface is shown in red. (C) The molecular model of the ARD of IκBζ. The protein is colored blue and the positions of the flexible amino acid residues determined by the molecular dynamic simulations are highlighted in red.
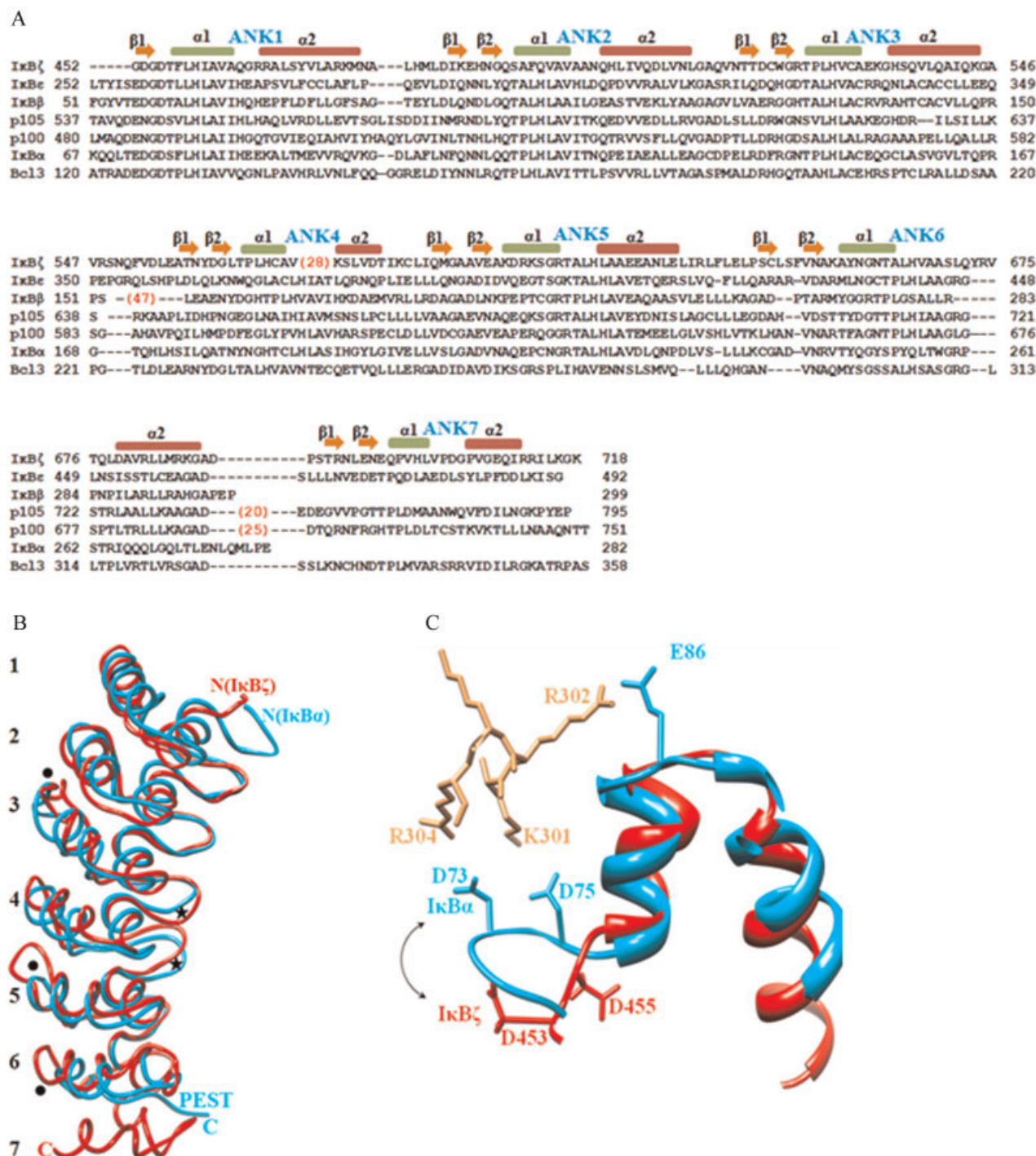
Figure 3. *Comparison of IκBζ and IκBα structures.* (A) Sequence alignment of IκBζ homologs. Secondary structure elements are indicated above the IκBζ. Large numbers of insertions in the IκBβ, IκBζ, p105 and p100 are indicated by numbers in parentheses. (B) Superimposition of the IκBζ and IκBα Cα backbones (Jacobs and Harrison, 1998). IκBζ and IκBα are shown in red and cyan, respectively. Differences between IκBζ (red) and IκBα (cyan) within the residues joining ANK repeats 3, 5, and 6 and in between the ANK repeats 3–4 and 4–5 are represented by dots and asterisks, respectively. (C) Differences between IκBζ (red) and IκBα (cyan) within ANK1. The conformational differences in the N-terminal residues are indicated by the double-headed arrow.

Structure refinement and stability evaluation

The constructed model was subjected to MD simulation to assess the stability of the model and to identify the energetically favorable structure for further evaluation of the protein–protein docking. The structural stability of the constructed model during the MD simulation was examined using the RMSD. The RMSD plot for the protein Cα atoms with reference to the initial structure as a function of time is shown in Figure 4A of the Supplementary Material (S4). In the thermodynamically equilibrated region, the trajectories do not show any significant changes. However, the superimposition of initial modeled structure with the final refined structure from the explicit solvent method revealed that there are structural rearrangements within the interhelical turn of ANK1, 6
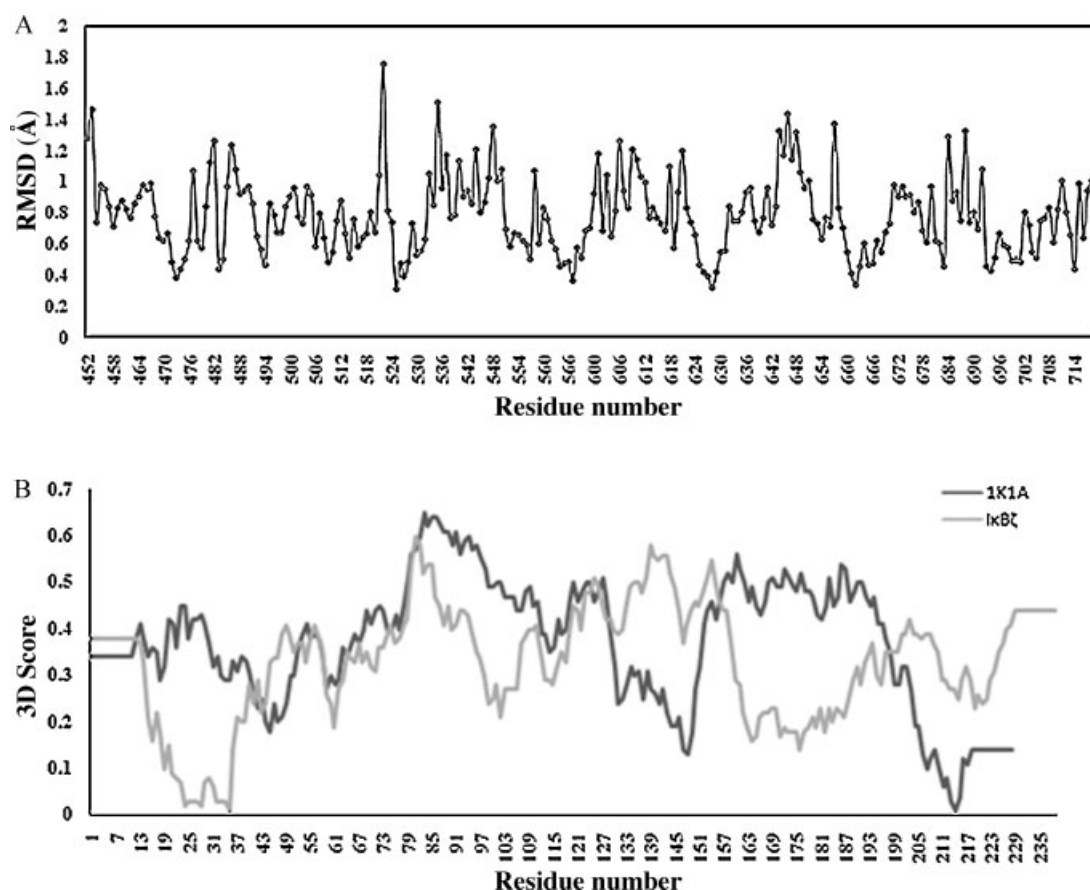
Copyright © 2010 John Wiley & Sons, Ltd.

Figure 4. *Identification of the flexible residues in IκBζ ARD.* (A) RMS deviations in individual amino acid residues of IκBζ during the last 2 ns of MD simulation trajectory. The amino acid residue numbers are plotted on the *X*-axis, while the RMS deviations (in Angstrom unit) are plotted on the *Y*-axis. (B) The 3D scores for the modeled IκBζ structure.

and 7 and also in between ANK repeats 1–2, 2–3, 3–4, 5–6, and 6–7 with the RMSD of 2.6 Å, which are represented as dots and asterisks, respectively (Figure S5 of the Supplementary Material). The structure closest to the average structure (see methods) was selected from the 5 ns MD simulation and subjected to further energy minimization for the fine refinement. This optimized model was subsequently assessed by PROCHECK and Verify3D server. The Ramachandran plot revealed that 97.1% of the φ–ψ dihedral angles were present in the most favorable regions, while the remaining 2.9% of residues were found within the allowed regions. The 3D structural profiles of both IκBζ and Bcl-3 produced by the Verify3D evaluation server are shown in Figure 4. Verify3D reported that IκBζ had no values below 0.03, which indicates that all residues were located in the favorable environment. The PROCHECK and Verify3D server results revealed that the optimized model is satisfactory, and is thus considered to be a reliable source for the rest of the study.

Identification of flexible residues in IκBζ

To examine the flexible regions of the model, we generated the average RMSD values for each residue backbone around the last 2 ns of both simulations. Here, those residues that deviated more than 1 Å were considered highly flexible elements of this protein. There were 40 residues with large RMSD values for IκBζ ARD. Of these residues, 3 were situated in ANK1 (Gly452, Asp453, and

Met477), 4 were in ANK2 (His481, Met482, Lys486, Glu487), 10 in ANK3 (Cys521, Trp522, Lys533, His535, Gln537, Gln540, Lys544, Val547, Arg548, and Ser549), 4 in ANK4 (Asn550, Thr558, Leu601, and Glu603), 6 in ANK5 (Lys606, Ile 609, Gln610, Met611, Lys618, and Lys621), 10 in ANK6 (Glu644, Leu645, Pro646, Ser647, Cys648, Leu649, Phe651, Tyr657, Arg684, and Asp688), and 3 in ANK7 (Arg692, Gln611 and Gly718). As anticipated, the loop regions of the model, especially in between the ANK (34 amino acid residues), were found to contribute to increasing fluctuations (Figure 2C), and this flexibility may mediate the binding of IκBζ to its partners.

IκBζ cofactor binds with the p50/p65 hetero and p50/p50 homodimer NF-κB subunits

We used GRAMM, a molecular docking program that uses shape complementarity to assess the interaction of protein molecules, to identify the likely binding sites of the p50/p65 hetero and p50/p50 homodimer interfaces for the cofactor/regulator, IκBζ. In addition to the available literature information (see methods), our comparative study clearly demonstrated that IκBζ has no association with p65 NLS, located near the DD. Since only the DNA binding domain is left in the RHD to interact with its partner, we assumed that the IκBζ binding should overlap with the DNA binding domain of the p65 subunits of NF-κB. This led to the model structure of the IκBζ-p50/p65 (Figure 5A) and IκBζ-p50/
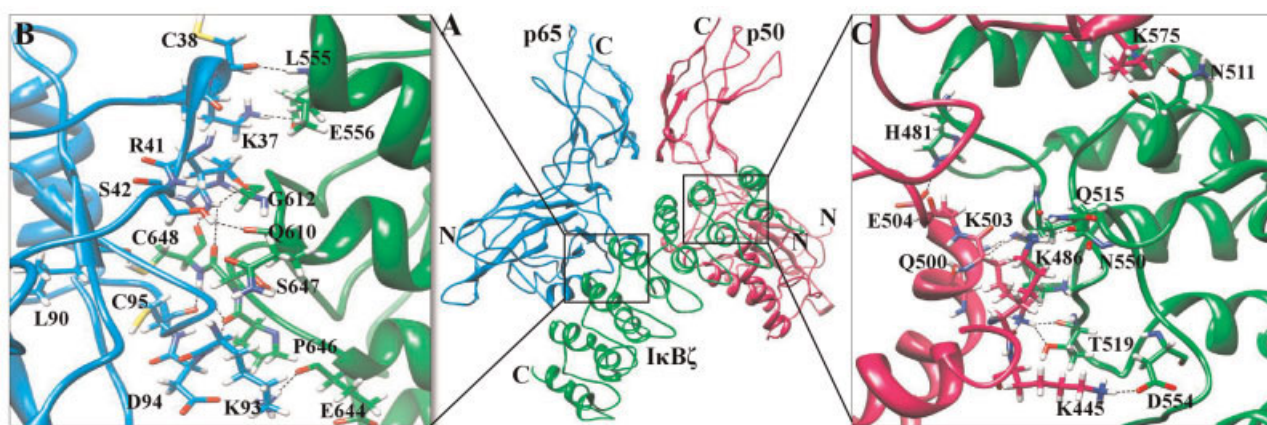
Figure 5. *Docking studies predict that the cofactor IκBζ ARD binds at the side of the p50/p65 heterodimer interface.* (A) The p50/p65 heterodimers, represented as a ribbon diagram, are shown in magenta and cyan, respectively. Docked IκBζ are represented as green in the ribbon diagram. (B) p65–IκBζ binding interface. Side chains of the amino acid contributing to the hydrogen bonding formation (marked as black) are represented by a stick model with the residue name and numbers shown next to them. (C) p50–IκBζ binding interface is also represented in similar fashion as in (B).

p50 homodimer complex (Figure 6A), in which there are several intermolecular hydrogen bonds and hydrophobic interactions between these two complexes that occur apart from the long range electrostatic interactions.

The buried surface at the interface of the IκBζ–p50/p65 heterodimer complex was separated from the p50/p65 heterodimer by 1457 Å^2 and from IκBζ by 1445 Å^2. The buried surface areas of the two partners (IκBζ–p50/p65 and p50/p65–IκBζ) had different values due to the difference in the number of residues present in the complex interface. The buried surface was in the range of typical physiological interaction surfaces. Based on the solvation energy calculated from the buried surface area and specific electrostatic interactions, the dimer interface was judged by the PROTORP server (Reynolds *et al.*, 2009) to constitute a physiological interaction. The DNA binding domain of p65 and

p50 contributed 24 and 21 residues, respectively, which made contacts (ΔASA > 1 Å^2) with 42 residues of IκBζ located in the region between ANK1–ANK5. As shown in Table 1, these residues produce the strongest van der Waals interactions (ΔASA > 40 Å^2) in the complex interface. The specific residues involved are Cys648 for IκBζ, Arg41 for p65 and Lys503 for p50. Twenty-two hydrogen bonds are present in the interface of the IκBζ–p50/p65 complex, of which 8 are donated by p65, 5 by p50, and 15 are inherited from IκBζ. IκBζ Cys648 forms 3 hydrogen bonds with Cys95, Leu90, and Arg41 of p65. Arg41 from p65 forms two and one hydrogen bond with IκBζ Ser647 and Gly612, respectively. In addition, IκBζ pro646, Thr519, Lys486, Gln515/Asn550, and Asn511 produce two hydrogen bonds with p65 Asp94/Cys95, p50 Lys503, p50 Gly500, p50 Lys444, and p50 Lys575, respectively (Figures 5B and 5C). Strong electrostatic interactions were also
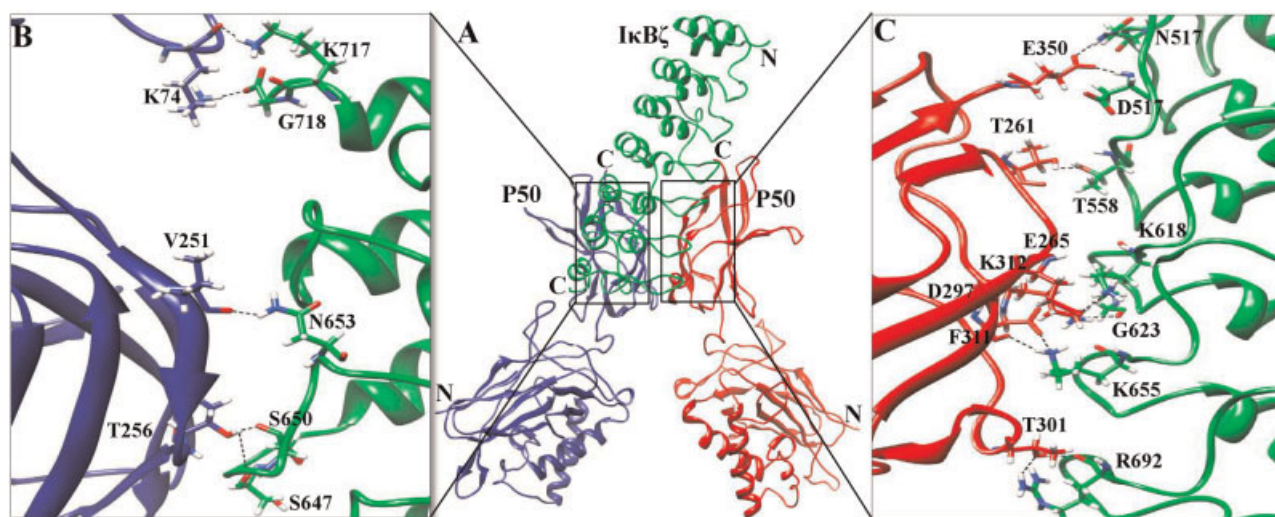
Figure 6. *IκBζ ARD–p50 homodimer interface.* (A) The p50/p50 dimers are blue and red in the ribbon diagram. Docked IκBζ are represented as green in the ribbon diagram. (B) The p50 (chain A)–IκBζ binding interface. Side chains of the amino acid contributing to the hydrogen bonding formation (marked as black color) are represented by a stick model with residue name and numbers shown next to them. (C) The p50 (chain B)–IκBζ binding interface is represented in a similar fashion as in (B).

Table 1. Residues that produce strong interactions (ΔASA > 40 Å^2) in the interface of the IκBζ–p50/p65 subunit of NF-κB

Residue number and type	NF-κB chain	ΔASA (Å^2)	Residue number and type in IκBζ chain	ΔASA (Å^2)
Arg35	A	40	Met477	75
Lys37	A	56	Leu480	103.3
Cys38	A	79.6	Met482	59
Glu39	A	56	Lys486	65.4
Arg41	A	87.5	Asn511	44.3
Lys93	A	64.5	Asn517	43.5
Arg187	A	43.8	Cys521	41
Lys444	B	97.5	Arg548	90.7
Lys445	B	43.3	Asp554	42.8
Val499	B	66	Glu556	46.1
Gln500	B	58.3	Gln610	42.6
Lys503	B	123.4	Gly612	52.9
Lys575	B	50.8	Cys648	130.3
Ser635	B	61	Leu649	53.4

Chain A and B indicate amino acids belonging to the p65 and p50 subunits, respectively.

Table 2. Residues that produce strong interactions (ΔASA > 40 Å^2) in the interface of the IκBζ–p50 homodimer of NF-κB

Residue number and type	NF-κb chain	ΔASA (Å^2)	Residue number and type in the IκBζ chain	ΔASA (Å^2)
Lys74	A	59.1	Asp554	42
Val251	A	48.4	Thr558	50
Arg252	A	72.4	Lys618	79.4
Thr256	A	65	Arg620	53.1
Pro344	A	57.7	Leu649	46.4
Leu346	A	44.2	Lys655	92.8
Thr261	B	48.9	Tyr657	45.6
Glu265	B	78.7	Arg692	73.1
Tyr267	B	41.4	Pro646	84.3
Glu297	B	57.5	Cys648	78.6
Ser299	B	47.5	Phe651	79.4
Thr301	B	78	Gly718	60
Lys312	B	73.3	Asp688	43.5
Glu350	B	100		

Chain A and B indicate amino acids belonging to p50 dimer subunits.

evident between the charged residues from both components of the complex. The strongest salt bridge was observed between IκBζ Arg548 and p65 Glu35. Additionally, ion pairs formed between IκBζ Glu553 and p65 Lys37, as well as between IκBζ Asp554 and p50 Lys445. The predicted binding surface (IκBζ–p50/p65) is large and constitutes 22 residues from IκBζ that form a complex with p50/p65 (Table 1 and Figure 5). Among these, 13 residues (Met477, His481, Met482, Lys486, Cys521, Arg548, Asn550, Gln610, Glu644, Pro646, Ser647, Cys648, and Leu649) are thermodynamically flexible. Such thermodynamically flexible residues identified in smad7 and CYBP61 have been shown to interact with their receptor and substrate, respectively, (Li *et al.*, 2004; Hariharan and Pillai, 2008), which further validates our docking model.

The interface of the IκBζ–p50/p50 dimer complex covered 1320 Å^2 from the p50 dimer and 1343 Å^2 from the IκBζ. The dimerization domain of p50 chain A and B contribute 28 and 14 residues, respectively, which form contacts (ΔASA > 1 Å^2) with 42 residues from IκBζ located in the region between ANK3–ANK7. As shown in Table 2, these residues produce strong van der Waals interactions (ΔASA > 40 Å^2) at the complex interface. The strongest interface residues were observed to be Lys656 for IκBζ and Glu350 for the p50 subunit. Fifteen hydrogen bonds were present at this interface, of which ten residues were donated by the p50 subunit and 12 from the IκBζ. This included a triple hydrogen bond between IκBζ Arg692 and p50 Thr301 and a double hydrogen bond between IκBζ Lys655 and p50 Asp297, respectively. In addition, IκBζ Ser647/Ser650, Lys717/Gly718, and Asn517/Asp554 were observed to form two hydrogen bonds with p50 Thr256, Lys74, and Glu350, respectively (Figures 6B and 6C). Furthermore, strong ionic interactions were observed between charged residues from both components in the complex. IκBζ Lys618 and Lys655 form ion pairs with p50 Glu265, Asp297, and Glu302, respectively. The present MD

approach demonstrated that 12 residues (Thr558, Lys618, Lys621, Pro646, Ser647, Cys648, Leu649, Phe651, Tyr657, Asp688, Arg692, and Gly718) from the above interface are thermodynamically flexible. Additionally, we asked whether the insertion (28 amino acids) plays any major role in the binding interface. To investigate this, we superimposed IκBζ (reported in Figure 1 of the Supplementary Material (S1)) with the final docked complexes (shown in Figures 5A and 6A). The results revealed that the deleted residues did not contribute to the binding interface (Figure 2 of the Supplementary Material (S2)).

We next used the FPSPD program to predict the functional sites in IκBζ. The functional patterns found in IκBζ were from residues 452–471 (ANK1), 478–494 (ANK2), 497–519 (ANK2 & 3), 600–632 (ANK4 & 5), 680–699 (ANK6), and 601–718 (ANK7). Patterns of 478–494, 497–519, and 600–632 were involved in binding with the p50/p65 complex (Table 1, Figures 5B and 5C). Conversely, the 600–632, 654–669, and 690–710 patterns were involved in binding with the p50 homodimer complex (Table 2, Figures 6B and 6C). Pattern 600–632 was found to contain residues that could interact with both hetero- and homodimers of NF-κB. Finally, pattern 452–471 was not found to contribute to any of the interactions identified in this study, but may be responsible for interactions with other cofactors such as CEBP during the transcriptional process (Yamazaki *et al.*, 2008).

Computational alanine scanning mutagenesis

The role played by individual amino acid side chains in the stabilization of the complex was further evaluated by computational alanine scanning studies, which identified the residues important for stabilization of the complex. This was conducted by determining the changes in the free energy of binding ($\Delta\Delta G$) that occur when various residues in the wild type

proteins are mutated to alanine (Kortemme and Baker, 2002; Kortemme *et al.*, 2004). The protocol captures the van der Waals, solvation, and hydrogen bonding contributions of interface residues involved in the binding. A positive value of $\Delta\Delta G$ implies that alanine mutations destabilize the complex, while a negative value indicates that alanine mutations have a stabilizing effect.

An approximate estimation of the individual contributions of the residues involved in the interaction could be obtained by computational methods. We used the Rosetta interface computational mutagenesis approach (Kortemme and Baker, 2002; Kortemme *et al.*, 2004), which is similar in principle to the experimental Ala-scanning mutagenesis protocol, to estimate the change in binding free energy ($\Delta\Delta G_{bind}$) that occurred when each residue at the interfaces of the IκBζ–p50/p65 and IκBζ–p50/p50 complex were mutated to Ala.

We utilized a cut-off of $\Delta\Delta G_{bind} > 1.0$ kcal/mol to qualitatively identify the hotspot residues essential for the interaction (Kortemme and Baker, 2002). A value of < -1.0 kcal/mol indicated that the mutation to Ala could stabilize the complex formation, whereas a value of >1.0 kcal/mol indicated desta-bilization of the complex. We observed that six IκBζ residues (Leu480, His481, Met482, Lys486, Arg548, and Glu556), five p65 residues (Arg35, Lys37, Glu39, Arg41, and Lys93) and four p50 residues (Lys444, Gln500, Lys503, and Lys575) were crucial for formation of the IκBζ–p50/p65 complex (Table 3), emphasizing their contribution to the complex stability. Conversely, evaluation of the second complex revealed that seven IκBζ residues

(Thr558, Glu619, Lys621, Phe651, Asn653, Arg692, and Gly718) and eight p50 homodimer residues (Arg255, Thr256, Thr261, Glu265, Thr301, Lys312, Leu246, and Glu350) were crucial for IκBζ–p50/p50 complex binding (Table 4). The rest of the residues at both complex interfaces had $\Delta\Delta G_{bind}$ values <0.8 kcal/mol, supporting the suggestion that their mutation to Ala may not have any functional consequences on complex formation.

DISCUSSION

Recent studies have suggested that the ARD of IκBζ can act as either positive (Yamamoto *et al.*, 2004; Motoyama *et al.*, 2005; Trinh *et al.*, 2008) or negative regulators (Totzke *et al.*, 2006) of TLR signaling. The present study was conducted to explain the molecular mechanism of the dual roles played by IκBζ with the help of modeling, dynamic simulation, and docking studies of the hetero- and homodimers of NF-κB. Sequence analysis of the IκBζ N-terminal region did not reveal any significant homology to proteins in the NCBI database. However, this region is known to be important for nuclear localization and transactivation activity (Motoyama *et al.*, 2005). The secondary structure prediction showed that the N-terminal region has no ANK repeats preceded by C-terminal ANK repeats. This type of architecture has also been reported in proteins such as the yeast ribosomal binding protein yar-1 (Lycan *et al.*, 1996).

The final IκBζ–p50/p65 inhibitory complex suggests that the residues of Arg35, Lys37, Cys38, Glu39, Arg41, Lys93, Gln119, and Arg187 from the p65 subunit are involved in the strongest interface of IκBζ (ANK4 & 5). Among these, Arg35 and Glu39 are known to be involved in the interaction with DNA bases, and Cys38 and Arg187 are involved in binding with the sugar phosphate backbone (Chen *et al.*, 1998b; Escalante *et al.*, 2002).

Table 3. The predicted contributions of residues as determined by virtual alanine scanning (IκBζ–p50/p65)

Residue number and type	Chain	Int_ID	$\Delta\Delta G$ (bind)	ΔG (partner)
Arg35	A	1	2.18	1.96
Lys37	A	1	1.35	−0.32
Glu39	A	1	2.11	2.08
Arg41	A	1	4.89	0.84
Lys93	A	1	1.26	−0.32
Lys444	B	1	1.56	−0.57
Gln500	B	1	2.72	−0.41
Lys503	B	1	1.45	1.14
Lys575	B	1	1.14	−0.46
Leu480	C	1	1.16	−0.17
His481	C	1	1.29	−0.09
Met482	C	1	1.02	0.34
Lys486	C	1	1.12	2.75
Arg548	C	1	2.04	−0.26
Glu556	C	1	1.38	0.95

Chain A denotes the p65 subunit; chain B denotes the p50 subunit; chain C denotes the IκBζ chain. Column 1: Mutated residues in the PDB file. Column 2: Chain, PDB chain identifier. Column 3: Int_ID, measure of whether a residue is interacting directly (1) or not interacting directly but buried upon binding (0). Column 4: $\Delta\Delta G$ (bind), predicted change in binding free energy upon alanine mutation. Column 5: ΔG (partner), predicted change in protein stability of the mutated partner upon alanine mutation.

Table 4. Results of the predicted contributions of residues through virtual alanine scanning (IκBζ–p50 dimer)

Residue number and type	Chain	Int_ID	$\Delta\Delta G$ (bind)	ΔG (partner)
Arg255	A	1	1.93	1.92
Thr256	A	1	1.02	0.89
Leu246	A	1	1.12	1.53
Thr261	B	1	1.36	0.36
Glu265	B	1	2.35	−0.04
Thr301	B	1	1.92	−0.28
Lys312	B	1	1.35	0.62
Glu350	B	1	1.45	−0.32
Thr558	C	1	0.92	0.68
Glu619	C	1	1.63	1.04
Lys621	C	1	4.77	0.84
Phe651	C	1	1.57	0.91
Asn653	C	1	1.00	0.47
Arg692	C	1	1.27	1.23
Gly718	C	1	1.96	−0.67

Chain A and B denote the p50 dimer and chain C denotes the p50 IκBζ subunit. The description of each column is the same as in Table 3.

Conversely, IκBζ (ANK1–3) interfaces with the p50 subunit residues Lys444, Lys445, Val499, Gln500, Lys503, Lys575, and Ser635. However, none of the p50 residues are involved in direct interaction with the bases of DNA. Furthermore, only two residues, Lys444 and Lys445, are involved in contact with the sugar phosphate backbone in the minor groove region (Chen *et al.*, 1998b). The region, which is where IκBζ associates with the DNA binding domain of the p50/p65 subunits, contains important amino acid residues that interact with the bases as well as the sugar phosphate backbone of DNA present in p65 but bind only with the sugar phosphate backbone of the p50 subunit. In fact, there will be no more p50/p65 subunits available to the promoter region, which will ultimately inhibit the transcription mediated by the p50/p65 subunit. Generally, p65 subunits contain the transactivation domain at the C-terminal end, which is important to its transcriptional activity (O'Shea and Perkins, 2008). IκBζ inhibits p65 transactivation activity through its binding with the N-terminal DNA binding domain.

Stimulation of TNFα makes cells more resistant to apoptosis by suppressing IκBζ, while over-expression of IκBζ is sufficient to induce cell death (Totzke *et al.*, 2006). However, this study could not identify the molecular mechanism of cell survival or apoptosis by IκBζ. The general mechanism of apoptosis from the available literature is as follows. Upon stimulation with TNFR1, complex I, which is composed of TNFR1 receptor along with TRADD, RIP1, TRAF2/5, c-IAP1 and probably other known or unidentified proteins, is rapidly assembled. This complex leads to activation of inhibitory NF-κB kinase (IKK) and Jun kinase (JNK) cascade. Activation of IKK leads to nuclear translocation of NF-κB along with upregulation of several anti-apoptotic genes, including the gene encoding for c-FLICE-inhibitory protein (c-FLIP), which is a specific inhibitor of caspase-8 activation. This further enhances the probability of cell survival, but not apoptosis. After some time, complex I becomes dissociated and a soluble complex II is formed, which, in addition to TRADD, RIP1, and TRAF2/5, recruits the adaptor protein (Fas-associated death domain protein; FADD). This complex can then activate caspase-8, which leads to the activation of apoptosis provided that the NF-κB signal from the complex I fails to induce the expression of antiapoptotic proteins such as c-FLIP (Micheau and Tschopp, 2003; Karin, 2006). Based on our current understanding from the present docking study, we suggest the following model. IκBζ inhibits NF-κB activation and results in inhibition of expression of antiapoptotic genes encoding c-FLIP. As a result, the complex II-mediated caspase-8 becomes activated and triggers cell apoptosis. Interestingly, studies have suggested that mouse IκBζ binds to NF-κB and prevents the TNFα promoter activation (Yamazaki *et al.*, 2001; Motoyama *et al.*, 2005). Since the TNFα promoter region requires p50/p65 subunits for its activation (Yao *et al.*, 1997), it may prove enlightening to determine why IκBζ overexpression inhibits TNFα production in mice. It is also important to mention that IκBζ is strongly up-regulated upon extracellular TLR ligand activation and acts as a negative feedback loop to provide an effective control mechanism for NF-κB activity in the nucleus.

Evaluation of the IκBζ–p50/p50 complex revealed that ANK3–ANK7 interact with the dimerization domain along with the nuclear localization signal of the p50 subunit. The obtained IκBζ–p50/p50 docked complex was in agreement with a previous surface plasmon resonance study (Trinh *et al.*, 2008). The binding orientation of IκBζ with this homodimer is similar to that of the classical IκBα–p50/p65 heterodimer (Huxford *et al.*, 1998). Although the IκB protein binding orientation is the same,

there might be differences in the regulation of NF-κB dependent gene expression by IκBα and IκBζ. Activation of p65-containing NF-κB heterodimer by LPS or IL-1 leads to the expression of NF-κB-dependent genes including IκBα and IκBζ. After translation, IκBα enters the nucleus, where it targets NF-κB dimers with p65 subunits and removes them from DNA through its PEST motif. In contrast, IκBζ enters the nucleus and targets the p50/p50 homodimer, which is already bound to a promoter region, thereby blocking transcription due to unavailability of the transactivation domain. Although overexpression experiments have suggested that IκBζ does exhibit transactivation potential when bound to p50, until this study there had been no report of a well-defined transactivation domain or transactivation activity for IκBζ (Motoyama *et al.*, 2005). Our structural studies suggest that the IκBζ and p50 homodimer complex is devoid of any PEST motif, which is also a major structural difference when compared to the corresponding IκBα–p50/p65 heterodimer-DNA. This absence of a PEST motif enables IκBζ to activate transcription.

The present MD study identified a total of 40 flexible residues. Among these, 25 were present in two different docking models and identified only four residues (P646, S647, Cys648, and Leu649) that were common in both the complexes. Recent reports suggest that once the stable ternary complex (IκBζ–p50 subunits) is formed, it acts as a hallmark for the recruitment of Brg1 and C/EBP (Yamazaki *et al.*, 2008). These 19 amino acids (Gly452, Asp453, Glu487, Leu601, Glu603, Trp522, Lys533, His535, Gln537, Gln540, Lys544, Val547, Ser549, Lys606, Ile609, Met611, Leu645, Arg684, and Gln611) do not participate in the above assembly, but may interact with Brg1 and C/EBP, thereby stabilizing the promoter binding. These residues can also interact with STAT3 and hence act as an inhibitor (Wu *et al.*, 2009). Although there were species-specific differences in the regulation of NF-κB by IκBζ, the results presented here document the high structural flexibility of IκBζ ARD, which arises mainly due to its longer loops and partly due to the possession of a greater number of thermodynamically flexible residues to interact with its partner. Taken together, these characteristics may offer an explanation of IκBζ dual functions.

CONCLUSION

In this study, we elucidated a 3D model for IκBζ ARD to show its dual function with homo- and heterodimers of NF-κB subunits. This data is helpful to understand the binding mechanism of IκBζ and its dual function as a positive and negative regulator during TLR signaling. This model can be utilized as a guide for the future experimental and computational studies to draw biological and functional conclusions.

REFERENCES

Chen FE, Huang DB, Chen YQ, Ghosh G. 1998a. Crystal structure of p50/p65 heterodimer of transcription factor NF-kappaB bound to DNA. *Nature* **391**(6665): 410–413.

Chen YQ, Ghosh S, Ghosh G. 1998b. A novel DNA recognition mode by the NF-kappa B p65 homodimer. *Nat. Struct. Biol.* **5**(1): 67–73.

Eisenberg D, Luthy R, Bowie JU. 1997. VERIFY3D: assessment of protein models with three-dimensional profiles. *Method. Enzymol.* **277**: 396–404.

Escalante CR, Shen L, Thanos D, Aggarwal AK. 2002. Structure of NF-kappaB p50/p65 heterodimer bound to the PRDII DNA element from the interferon-beta promoter. *Structure* **10**(3): 383–391.

Forrer P, Stumpp MT, Binz HK, Pluckthun A. 2003. A novel strategy to design binding molecules harnessing the modular nature of repeat proteins. *FEBS Lett.* **539**(1–3): 2–6.

Gaudet R. 2008. A primer on ankyrin repeat function in TRP channels and beyond. *Mol. Biosyst.* **4**(5): 372–379.

Ghosh G, van Duyne G, Ghosh S, Sigler PB. 1995. Structure of NF-kappa B p50 homodimer bound to a kappa B site. *Nature* **373**(6512): 303–310.

Ghosh S, May MJ, Kopp EB. 1998. NF-kappa B and Rel proteins: evolutionarily conserved mediators of immune responses. *Annu. Rev. Immunol.* **16**: 225–260.

Hariharan R, Pillai MR. 2008. Structure-function relationship of inhibitory Smads: structural flexibility contributes to functional divergence. *Proteins* **71**(4): 1853–1862.

Haruta H, Kato A, Todokoro K. 2001. Isolation of a novel interleukin-1-inducible nuclear protein bearing ankyrin-repeat motifs. *J. Biol. Chem.* **276**(16): 12485–12488.

Hatada EN, Krappmann D, Scheidereit C. 2000. NF-kappaB and the innate immune response. *Curr. Opin. Immunol.* **12**(1): 52–58.

Hayden MS, Ghosh S. 2004. Signaling to NF-kappaB. *Genes Dev.* **18**(18): 2195–2224.

Hayden MS, Ghosh S. 2008. Shared principles in NF-kappaB signaling. *Cell* **132**(3): 344–362.

Huxford T, Huang DB, Malek S, Ghosh G. 1998. The crystal structure of the IkappaBalpha/NF-kappaB complex reveals mechanisms of NF-kappaB inactivation. *Cell* **95**(6): 759–770.

Jacobs MD, Harrison SC. 1998. Structure of an IkappaBalpha/NF-kappaB complex. *Cell* **95**(6): 749–758.

Jones S, Thornton JM. 1996. Principles of protein-protein interactions. *Proc. Natl Acad. Sci. USA* **93**(1): 13–20.

Karin M. 2006. Nuclear factor-kappaB in cancer development and progression. *Nature* **441**(7092): 431–436.

Kitamura H, Kanehira K, Shiina T, Morimatsu M, Jung BD, Akashi S, Saito M. 2002. Bacterial lipopolysaccharide induces mRNA expression of an IkappaB MAIL through toll-like receptor 4. *J. Vet. Med. Sci.* **64**(5): 419–422.

Kitamura H, Kanehira K, Okita K, Morimatsu M, Saito M. 2000. MAIL, a novel nuclear I kappa B protein that potentiates LPS-induced IL-6 production. *FEBS Lett.* **485**(1): 53–56.

Kortemme T, Baker D. 2002. A simple physical model for binding energy hot spots in protein-protein complexes. *Proc. Natl Acad. Sci. USA* **99**(22): 14116–14121.

Kortemme T, Kim DE, Baker D. 2004. Computational alanine scanning of protein-protein interfaces. *Sci. STKE* **2004**(219): p. l2.

Lee B, Richards FM. 1971. The interpretation of protein structures: estimation of static accessibility. *J. Mol. Biol.* **55**(3): 379–400.

Li X, Baudry J, Berenbaum MR, Schuler MA. 2004. Structural and functional divergence of insect CYP6B proteins: from specialist to generalist cytochrome P450. *Proc. Natl Acad. Sci. USA* **101**(9): 2939–2944.

Lovell SC, Davis IW, Arendall WB 3rd, de Bakker PI, Word JM, Prisant MG, Richardson JS, Richardson DC. 2003. Structure validation by Calpha geometry: phi,psi and Cbeta deviation. *Proteins* **50**(3): 437–450.

Lycan DE, Stafford KA, Bollinger W, Breeden LL. 1996. A new Saccharomyces cerevisiae ankyrin repeat-encoding gene required for a normal rate of cell proliferation. *Gene* **171**(1): 33–40.

Main ER, Jackson SE, Regan L. 2003. The folding and design of repeat proteins: reaching a consensus. *Curr. Opin. Struct. Biol.* **13**(4): 482–489.

Malek S, Huxford T, Ghosh G. 1998. Ikappa Balpha functions through direct contacts with the nuclear localization signals and the DNA binding sequences of NF-kappaB. *J. Biol. Chem.* **273**(39): 25427–25435.

Micheau O, Tschopp J. 2003. Induction of TNF receptor I-mediated apoptosis via two sequential signaling complexes. *Cell* **114**(2): 181–190.

Michel F, Soler-Lopez M, Petosa C, Cramer P, Siebenlist U, Muller CW. 2001. Crystal structure of the ankyrin repeat domain of Bcl-3: a unique member of the IkappaB protein family. *EMBO J.* **20**(22): 6180–6190.

Miguel RN. 2004. Sequence patterns derived from the automated prediction of functional residues in structurally-aligned homologous protein families. *Bioinformatics* **20**(15): 2380–2389.

Mosavi LK, Cammett TJ, Desrosiers DC, Peng ZY. 2004. The ankyrin repeat as molecular architecture for protein recognition. *Prot. Sci.* **13**(6): 1435–1448.

Motoyama M, Yamazaki S, Eto-Kimura A, Takeshige K, Muta T. 2005. Positive and negative regulation of nuclear factor-kappaB-mediated transcription by IkappaB-zeta, an inducible nuclear protein. *J. Biol. Chem.* **280**(9): 7444–7451.

O'Shea JM, Perkins ND. 2008. Regulation of the RelA (p65) transactivation domain. *Biochem. Soc. Trans.* **36**: (Pt 4): 603–608.

Pettersen EF, Goddard TD, Huang CC, Couch GS, Greenblatt DM, Meng EC, Ferrin TE. 2004. UCSF Chimera–a visualization system for exploratory research and analysis. *J. Comput. Chem.* **25**(13): 1605–1612.

Ponder JW, Case DA. 2003. Force fields for protein simulations. *Adv. Prot. Chem.* **66**: 27–85.

Reynolds C, Damerell D, Jones S. 2009. ProtorP: a protein-protein interaction analysis server. *Bioinformatics* **25**(3): 413–414.

Richmond TJ. 1984. Solvent accessible surface area and excluded volume in proteins. Analytical equations for overlapping spheres and implications for the hydrophobic effect. *J. Mol. Biol.* **178**(1): 63–89.

Rogers S, Wells R, Rechsteiner M. 1986. Amino acid sequences common to rapidly degraded proteins: the PEST hypothesis. *Science* **234**(4774): 364–368.

Sedgwick SG, Smerdon SJ. 1999. The ankyrin repeat: a diversity of interactions on a common structural framework. *Trend. Biochem. Sci.* **24**(8): 311–316.

Siebenlist U, Franzoso G, Brown K. 1994. Structure, regulation and function of NF-kappa B. *Annu. Rev. Cell Biol.* **10**: 405–455.

Tina KG, Bhadra R, Srinivasan N. 2007. PIC: Protein Interactions Calculator. *Nucleic Acids Res.* **35** (Web Server issue): W473–W476.

Totzke G, Essmann F, Pohlmann S, Lindenblatt C, Janicke RU, Schulze-Osthoff K. 2006. A novel member of the IkappaB family, human IkappaB-zeta, inhibits transactivation of p65 and its DNA binding. *J. Biol. Chem.* **281**(18): 12645–12654.

Tovchigrechko A, Vakser IA. 2006. GRAMM-X public web server for protein-protein docking. *Nucleic Acids Res.* **34** (Web Server issue): W310–W314.

Trinh DV, Zhu N, Farhang G, Kim BJ, Huxford T. 2008. The nuclear I kappaB protein I kappaB zeta specifically binds NF-kappaB p50 homodimers and forms a ternary complex on kappaB DNA. *J. Mol. Biol.* **379**(1): 122–135.

Wu Z, Zhang X, Yang J, Wu G, Zhang Y, Yuan Y, Jin C, Chang Z, Wang J, Yang X, He F. 2009. Nuclear protein IkappaB-zeta inhibits the activity of STAT3. *Biochem. Biophys. Res. Commun.* **387**(2): 348–352.

Yamamoto M, Yamazaki S, Uematsu S, Sato S, Hemmi H, Hoshino K, Kaisho T, Kuwata H, Takeuchi O, Takeshige K, Saitoh T, Yamaoka S, Yamamoto N, YamamotoS, Muta T, Takeda K, Akira S. 2004. Regulation of Toll/IL-1-receptor-mediated gene expression by the inducible nuclear protein IkappaBzeta. *Nature* **430**(6996): 218–222.

Yamazaki S, Muta T, Matsuo S, Takeshige K. 2005. Stimulus-specific induction of a novel nuclear factor-kappaB regulator, IkappaB-zeta, via Toll/Interleukin-1 receptor is mediated by mRNA stabilization. *J. Biol. Chem.* **280**(2): 1678–1687.

Yamazaki S, Matsuo S, Muta T, Yamamoto M, Akira S, Takeshige K. 2008. Gene-specific requirement of a nuclear protein, IkappaB-zeta, for promoter association of inflammatory transcription regulators. *J. Biol Chem.* **283**(47): 32404–32411.

Yamazaki S, Muta T, Takeshige K. 2001. A novel IkappaB protein, IkappaB-zeta, induced by proinflammatory stimuli, negatively regulates nuclear factor-kappaB in the nuclei. *J. Biol. Chem.* **276**(29): 27657–27662.

Yao J, Mackman N, Edgington TS, Fan ST. 1997. Lipopolysaccharide induction of the tumor necrosis factor-alpha promoter in human monocytic cells. Regulation by Egr-1, c-Jun, and NF-kappaB transcription factors. *J. Biol. Chem.* **272**(28): 17795–17801.